Perspective on active submillimeter electromagnetic wave imaging using CMOS integrated circuits technologies 🅕✅

Kenneth K. O ✉ ; Wooyeol Choi ; Ruonan Han

Check for updates

View Online   Export Citation   CrossMark

AIP Publishing

Perspective on active submillimeter electromagnetic wave imaging using CMOS integrated circuits technologies Ⓕ

View Online   Export Citation   CrossMark

Kenneth K. O,[1,a)] Ⓘ Wooyeol Choi,[2] Ⓘ and Ruonan Han[3] Ⓘ

AFFILIATIONS

[1]Texas Analog Center of Excellence & Department of ECE, University of Texas at Dallas, Richardson, Texas 75080, USA
[2]School of Electrical and Computer Engineering, Oklahoma State University, Stillwater, Oklahoma 74078, USA
[3]Department of Electrical and Computer Science, Massachusetts Institute of Technology, Cambridge, Massachusetts 02139, USA

[a)]Author to whom correspondence should be addressed: k.k.o@utdallas.edu

ABSTRACT

The performance of CMOS transmitters and receivers operating at the submillimeter electromagnetic wave frequencies have sufficiently improved for use in active transmission and reflection-mode imaging applications that have the potential for broad deployment and utilization. Imaging integrated circuits have the potential to be large in area to support a high number of pixels along with digital backend processing circuits. For high volume imaging applications that may eventually be included in automobiles, smartphones, laptops, tablets, and others, a large manufacturing capacity to support the volume of large area ICs is necessary. For this, the use of CMOS technologies with a much larger manufacturing capacity is favored. It should be possible to improve the performance of CMOS circuits to increase the range, and operation margin and frequency. The electronically steerable submillimeter-wave reflector technology holds the promise for improving the performance and energy efficiency of submillimeter-wave imaging systems by multiple orders of magnitude, and it is a critical research area. Increasing the operating frequency from 430 to 850 GHz using CMOS integrated circuits to improve the angular resolution by 2X at a given form factor (∼0.15° for a reflector diameter of 15 cm) can make the submillimeter-wave imaging competitive to the LIDAR angular-resolution performance, while providing superior capabilities in visually impaired conditions and making the imaging devices more affordable.

I. INTRODUCTION

Imaging[1–5] has been one of the most widely studied and fascinating submillimeter electromagnetic or terahertz wave applications. Absorption, reflection, and transmission of the submillimeter waves are highly material dependent, and these dependences provide contrast in images. This modality can be used to image through walls for locating wires and pipes; through materials to detect defects such as air voids, cracks, knots, and others; and through poor visibility weather conditions such as fog, rain, and dust as well as through smoke and fire. These capabilities, however, are not broadly utilized. A key barrier for this has been the availability of low-cost electronics with sufficient performance and power efficiency that can be used to construct compact and affordable imaging systems. The advances of high frequency capabilities of the mainstream Silicon IC technologies which are utilized to manufacture the components in almost every affordable electronics systems have made implementation of integrated circuits for submillimeter-wave imaging using the technologies, more specifically, CMOS (Complementary Metal Oxide Semiconductor) and SiGe HBT (Heterojunction Bipolar Transistor) technologies an active area of research. Imaging integrated circuits have the potential to be large in area to support a large number of pixels along with digital backend processing circuits. For high volume applications that may eventually be included in automobiles, smartphones, laptops, tablets, and others, a large manufacturing capacity to support the volume of large area ICs is necessary, and the use of CMOS with a much larger manufacturing capacity and associated lower cost than that of SiGe HBT technologies is favored. This has also been the reason why the manufacturing of Wi-Fi, smartphone, and 77-GHz radar ICs shifted to using CMOS technologies from

SiGe HBT technologies. For these, this paper focuses on submillimeter-wave imaging circuits that can be fabricated in CMOS.

This paper more specifically reviews the state of art for the submillimeter-wave CMOS circuit performance as well as key imaging demonstrations using CMOS integrated circuits. Furthermore, this paper presents perspectives on how these capabilities could be utilized to address submillimeter-wave imaging applications that have the potential for broad deployment as well as directions for future efforts. The state of art for the signal power generation, and noise equivalent power (NEP) as well as noise figure of imaging pixels that can be realized using CMOS integrated circuits technologies are reviewed in Sec. II. These determine the signal-to-noise ratio (SNR) of detected signals, which is a key performance metric for active imaging systems. This is followed in Sec. III by an overview of active transmission-mode imaging, and discussions of system concepts with potential for wide utilization that can be supported by the state-of-art performance. The same as well as future research directions for active reflection-mode imaging are discussed in Sec. IV. Lastly, the paper is concluded in Sec. V.

II. CMOS SUBMILLIMETER-WAVE CIRCUIT PERFORMANCE

Active imaging systems require a source/transmitter to illuminate targets and a detector/receiver to detect and analyze the signals reflected by or transmitted through targets. Although the end-to-end SNR varies dependent on system design such as the size of the array and external optics, it is fundamentally bounded by the output power of the signal source/transmitter that illuminates targets, and the minimum detectible signal of the detector or receiver that detects the signals scattered by the targets which, in turn, are limited by NEP and noise figure. The first CMOS sources operating at the submillimeter-wave frequencies more specifically at 320[6] and 410 GHz[7] were simultaneously reported in 2008. The first report of CMOS submillimeter-wave incoherent (amplitude detection) detector followed later in 2008 as part of a 600-GHz NMOS transistor focal plane array (FPA).[8] Since then, the performance and functional capabilities of submillimeter-wave or terahertz CMOS circuits and systems including that for signal generation and detection have rapidly advanced, and now it is possible to support practical imaging applications using CMOS circuits. In this section, the state-of-the-art performances for CMOS sources/transmitters and detectors/receivers are reviewed in the context of active imaging applications. The majority of these sources and detectors operating at frequencies near 300 GHz and above utilizes on-chip antennas, and the losses associated with the antennas are incorporated as part of the source and detector performance.

A. Output power of CMOS sources/transmitters

The upper limit of output frequency for sources implemented using active devices is set by the maximum oscillation frequency (f_{max}), the frequency at which the maximum available power gain becomes unity. Scaling down the dimensions of transistors typically increases their f_{max}. However, for the transistors in CMOS processes because of the increase in device parasitic series resistance resulting from scaling the transistors for low DC power

consumption and density, as well as the slower scaling of transistor and interconnect parasitic capacitances, f_{max} plateaued at around ~350 GHz when connected to the top metal level at which connections to passive components are typically made.[9] This occurred somewhere between the 65-nm and 22-nm technology nodes and makes fundamental signal generation and amplification in CMOS at frequencies above 300 GHz challenging. Fortunately, the performance of transmission-line based matching networks[10] and on-chip antennas[11] fabricated in CMOS improves with operating frequency up to ~1 THz. This helps to mitigate the performance degradation of circuits due to that for active devices with operating frequency.

To overcome this limitation, higher-order harmonic generation based on self-multiplication using switching actions or device nonlinearity is being utilized. The signal generation circuits can be categorized into oscillator-based and multiplier-based ones. The first one employs oscillators whose waveform is rich in harmonics or anharmonic oscillators. The harmonic generation can be performed using the inherent nonlinearity of devices in oscillators[7] or mixing devices directly integrated into oscillators.[6,12,13] The second approach relies on the more traditional amplifier-multiplier chain configuration, where a high-power signal at a fundamental frequency drives a frequency multiplier using active or passive nonlinear devices to generate outputs at higher-order harmonic frequencies.

The anharmonic oscillator-based approach is advantageous in overall power efficiency and circuit area because the fundamental signal generation and harmonic extraction are tightly integrated without external inputs. A DC-to-total RF power efficiency of 0.23% is achieved at 290 GHz[14] using a 65-nm CMOS process, and 0.08% at 587 GHz using a 40-nm CMOS process.[13] Also, the small size of the oscillator-based generation circuits enables large-scale 2D integration. In fact, 36 anharmonic oscillators are coupled to generate a total-radiated power of 0 dBm at 587 GHz.[15] On the other hand, the multiplier-based approach allows independent optimization of the fundamental signal generation and frequency multiplication, making it easier to achieve a wider output frequency range and higher-order multiplication. A 1.3-THz signal with an output power of −23 dBm has been generated by cascading a 650-GHz frequency quintupler and a 1.3-THz frequency doubler using MOS varactors in 65-nm CMOS.[16] The measurement setup-limited operation frequency range is 11% of its output center frequency, whereas that of anharmonic oscillators is limited to 5.3% at about half the output frequency of 694 GHz.[17]

Figure 1 depicts the output power of sources/transmitters fabricated using CMOS devices. The present state-of-art output power of CMOS signal generators using anharmonic oscillators with a frequency multiplication circuit is ~−1 dBm at 300 GHz,[14] ~−8 dBm at 482 GHz,[18] and −18 dBm at 694 GHz.[17] A transistor frequency multiplier is used to generate 0 dBm at 288 GHz,[19] and MOS varactor frequency multipliers are used to generate −3.2 dBm at 447 GHz,[20] −8 dBm at 480 GHz,[21] and −23 dBm at 1.33 THz.[16] The state of art for output power of CMOS sources in 2008 was ~−20 dBm at 190 GHz,[22] ~−46 dBm at 320 GHz,[6] and ~−49 dBm at 410 GHz.[7] The power generation at the submillimeter-wave frequencies using CMOS has indeed spectacularly advanced over the past 15 years. The linear fit of the highest power levels for unit
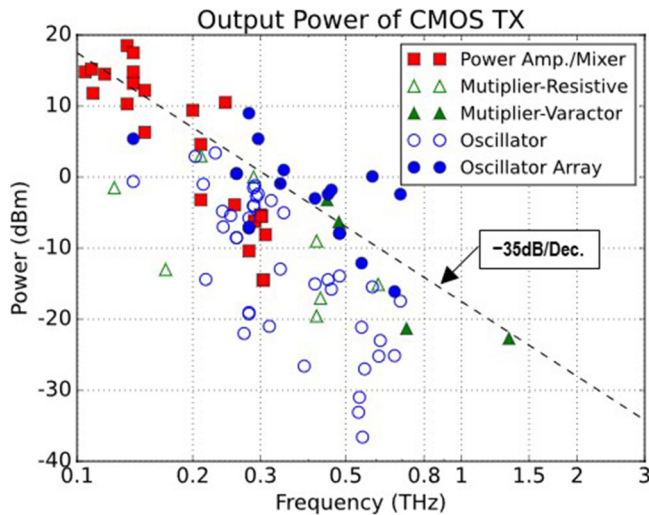
FIG. 1. Output power of signal sources in CMOS technologies using power amplifiers, mixers, resistive (transistor and diodes) and varactor frequency multipliers, oscillators, and oscillator arrays. The output power decreases ∼35 dB when the operating frequency is increased by a factor of 10. The references for the points in the figure can be found at https://www.wchoi.net/thz.

signal generators in Fig. 1 decreases ∼35 dB per decade with frequency. The fundamental signal amplification using CMOS technologies is limited to ∼300 GHz,[23,24] while the harmonic-based transmitters deliver superior output power at frequencies near and beyond 300 GHz. Frequency multipliers operate at higher frequencies and exhibit higher unit output power compared to that of anharmonic oscillators. The anharmonic oscillators and frequency multipliers can be arrayed to generate higher output power using spatial power combining. The efforts for arraying anharmonic oscillators are further along and as seen in Fig. 1 have led to the generation of higher total output power. Multiple high-power sources using the MOS transistor nonlinearity for frequency multiplication[15,17,19] rely on signal swings well above the limits recommended by the CMOS foundries. This is a concern and studies are needed to better understand the lifetime implications.

B. Noise performance of CMOS receivers

As mentioned, the performance of active imaging systems can be evaluated by the signal-to-noise ratio (SNR) of signal at a detector output. The key factor besides the source output power that determines the SNR is the minimum detectible signal of the detector or receiver that detects the signals scattered by targets. This section presents the state-of-art performance of CMOS detectors/receivers. Detectors/receivers for active imaging can be categorized into that use incoherent and that use coherent detectors.

Incoherent detectors use electronic devices to capture time varying amplitude of incoming signals. The detection process typically involves second-order nonlinearity to self-mix the incoming signal. Incoherent detectors can be as simple as one antenna coupled to a nonlinear device that can easily be integrated to form

large-scale arrays. NMOS transistors,[25,26] p–n diodes,[27] and Schottky barrier diodes (SBDs)[28,29] in CMOS have been used for detection of submillimeter-wave signals. Detection with a voltage responsivity (R_V [V/W]) of greater than 1 V/W up to ∼4 THz using an NMOS cold-FET detector[30] and detection with R_V of 25 V/W at 9.74 THz using a Schottky barrier diode in CMOS[31,32] have been demonstrated. Like CMOS pixels for visible light imagers, antenna-coupled incoherent detectors can be arranged to construct two-dimensional arrays, since they require one RF input connected to an antenna and one baseband output. Incoherent detector arrays with the necessary circuitry for amplification and pixel selection for imaging are demonstrated using cold-FET,[33,34] Schottky barrier diodes (SBDs),[35] and diode-connected FETs[28] in CMOS. However, the sensitivity of incoherent detectors is limited since the output level is proportional to the square of the input signal level that is small.

Coherent detectors, on the other hand, mix an input signal at RF with a local oscillator (LO) signal to perform frequency down-conversion or frequency translation to a lower frequency while retaining the phase information of input signal. The output signal amplitude of coherent detectors is linearly proportional to that of the input signal. Because the local oscillator signal is much larger than the input signal, coherent detection provides multiple orders of magnitude improved sensitivity compared to that of incoherent detectors. The minimum detectible signal (MDS) for mixer-based coherent detectors is $MDS = kT \times B \times F \times SNR_{min}$, where kT is the thermal noise floor, B is the noise bandwidth, F is the noise factor, and SNR_{min} is the minimum required SNR at the output. The equivalent for incoherent detectors is $MDS = NEP \times \sqrt{B} \times SNR_{min}$, where NEP is the noise equivalent power. Therefore, if the same signal bandwidth is assumed, $NEPs$ of incoherent detectors and NF of coherent detectors can be compared using these MDS expressions. An NEP can also be converted to an effective noise figure $[10log(NEP/(kT\sqrt{BW})]$. Figure 2 shows the double side band (DSB) noise figure $[10log(F)]$ of coherent receivers and the effective DSB noise figure of incoherent detectors as well as the effective NEP of coherent detectors and NEP of incoherent detectors fabricated in CMOS. A noise bandwidth of 1 kHz is assumed for the effective noise figure and effective NEP conversions.

The effective noise figures of incoherent receivers vary from 70 to 100 dB which as expected are significantly higher than that of coherent receivers, especially at frequencies below 1 THz. Coherent detection up to 1.2 THz has been demonstrated in CMOS.[36] The lowest measured DSB noise figures for CMOS receivers are 11 dB at 260 GHz[37] and 14 dB at 420 GHz.[38] Noise figures increase with a slope of ∼15 dB per decade as the output frequency is increased. This is significantly slower than the degradation for the output power of transmitters. At frequencies above 420 GHz, noise figures of CMOS circuits increase with a slope of ∼70 dB/decade due to the use of higher order subharmonic mixing.[28,39,40] The amplitude of LO (local oscillator) signal generated by frequency multiplication within coherent detectors/mixers is not sufficiently high to properly switch devices due to the increased loss of high-order frequency multiplication and operating frequency. This limitation can be mitigated using a separate frequency multiplier that is more efficient and can generate higher power, and by lowering the order of subharmonic mixing.
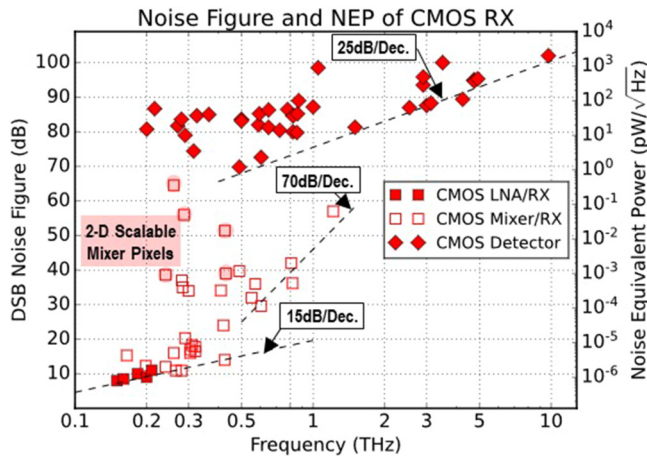
FIG. 2. Double sideband (DSB) noise figure of coherent receivers (LNA/RX: Low Noise Amplifier/Receiver, Mixer/RX: Mixer first receiver) and equivalent noise figure of incoherent detectors, as well as equivalent noise equivalent power (NEP) of coherent receivers and NEP of incoherent detectors when the noise bandwidth is 1 kHz. The noise performance of coherent receivers is significantly better than that of incoherent receivers up to ~1 THz. The references for the data included in the figure can be found at https://www.wchoi.net/thz.

Clearly, coherent detectors can achieve orders of magnitude better MDS for the same required SNR_{min}. Incoherent detector circuits can be made to act as a coherent detector by optically providing an LO signal. This can improve the equivalent sensitivity by more than 10 dB.[41] However, optically providing an LO signal greatly increases the system complexity. To overcome this, the LO circuits should be integrated into detector arrays. An LO distribution network is integrated to drive an eight-element array at 320 GHz, achieving 10-dB improved sensitivity compared to incoherent detectors.[42] An LO generation circuit is directly integrated with mixing devices to achieve a smaller footprint while supporting two-dimensional scalability.[43,44] Figure 2 also highlights the performance of 2D scalable coherent pixels. The 1×3 imaging pixel array fabricated in 65-nm CMOS[45] reported a DSB noise figure of 39 dB at 430 GHz and effective noise equivalent power of 1 fW/$\sqrt{Hz}$. The noise figure is 30-dB better than the effective noise figure of incoherent detectors operating at the same frequency range.

The first reported submillimeter-wave incoherent detector in CMOS operating at 600 GHz achieved the minimum NEP of ~400 pW/$\sqrt{Hz}$.[8] Since then, as can be inferred from Fig. 2, the noise performance of CMOS submillimeter-wave imaging pixels using incoherent detectors like the output power capabilities has dramatically improved. The lowest NEP approaching ~10 pW/$\sqrt{Hz}$ has been demonstrated using an 820-GHz NMOS pixel.[26] The effective NEP is reduced by multiple orders of magnitudes beyond that for incoherent detectors employing pixels with coherent detectors that utilize a mixer.[46,47] Coherent detectors can achieve an effective NEP below 1 fW/$\sqrt{Hz}$.[47]

These improvements of source/transmitter output power and detector/receiver NEP/noise figure greatly increased flexibility to construct capable transmission-mode and reflection-mode imaging

systems that can support a wide variety of applications. More importantly, the emergence of 77-GHz automotive radar applications[48,49] including imaging[50] using CMOS integrated circuits and commercial interests for 140-GHz radar imaging systems[51] provide the basis for extrapolation toward broad deployment of submillimeter-wave radar imaging devices that can support an angular-resolution capability of less than 0.3° (Ref. 45) which overlaps with that of LIDARs while satisfying the form factor requirements of automotive applications. Such imaging systems compared to LIDARs also hold promise for superior performance in visually impaired conditions, such as fog, dust, smoke, fire and others, lower power consumption, and ~10X lower cost.

III. ACTIVE TRANSMISSION-MODE IMAGING

The active transmission-mode imaging, in which a submillimeter-wave source and a detector are placed on the two sides of an object [Fig. 3(a)], can be employed to image over a short distance for parcel security screening, packing verification, monitoring drying processes, defects in ceramics and wood products, and many others. A 280-GHz transmission-mode imaging system using an 1D array of 256 plasmonic detectors fabricated on GaAs substrates with an NEP of 1 nW/$\sqrt{Hz}$ and a 140-GHz IMPATT source coupled to a frequency doubler with an output power at 280 GHz of ~40 mW is commercially available.[52] Typically, optical lenses/reflectors are used for beam collimation and focus so that most of the transmitted power can be directed to the object and detectors. The corresponding relaxed source power requirement makes silicon-based implementations practical. Thanks to the large aperture size of the optics, the lateral resolution of such transmission-mode imaging can be ~2 mm.

The first transmission-mode image formed using a detector array incorporating an on-chip folded dipole antenna fabricated in CMOS was reported in 2008. The detector array used to form images at 650 GHz employed a MOS transistor as the rectifying element.[53,54] The sub-100-pW/$\sqrt{Hz}$ NEP provided by square-law detectors fabricated in CMOS is significantly better than the 1-nW/$\sqrt{Hz}$ NEP of the plasmonic detectors used in the commercially available terahertz image sensors.[54] The CMOS source operating at frequencies near 280 GHz with the highest power generates around 9 dBm.[55] Though this power is lower than the 16-dBm of the IMPATT 280-GHz source,[52] a full CMOS implementation should support a higher SNR due to more than 10X lower NEP of CMOS detectors. Furthermore, CMOS implementation allows integration of amplifier banks and pixel control circuits along with a pixel array[26,33–35] to make the imager operation more robust as well as making the detector arrays more affordable and easier to use. Figure 4 shows such an array composed of 8×8 820-GHz diode-connected NMOS transistor detectors that can be individually addressed.[26] The detectors incorporate an on-chip patch antenna with a simulated efficiency of 74%. The outputs are amplified by an on-chip low noise amplifier with input referred noise of 2 nV/$\sqrt{Hz}$. The array exhibits the mean NEP of 36 pW/$\sqrt{Hz}$. The 2×1.75 mm^2 array can be easily scaled up to 10×10 mm^2 to include more than 40×40 elements. The arrays can also be designed so that they can be tiled to create a much larger detector array. As a matter of fact, a 32×32 1-THz focal plane array fabricated in
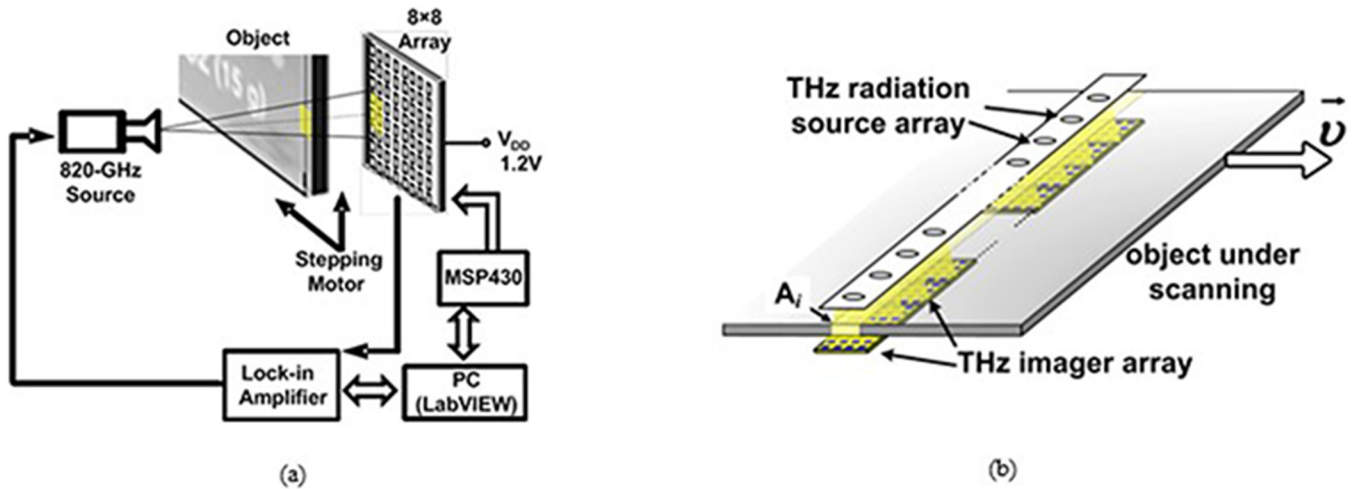
FIG. 3. (a) Transmission-mode imaging laboratory setup for an 8 × 8 array of 820-GHz diode-connected NMOS transistor detectors using an on-chip patch antenna with an on-chip bank of low noise amplifiers. From Kim *et al.*, IEEE Trans. Terahertz Sci. Technol. **6**(2), 306–317 (2016). Copyright 2016 Author(s), licensed under a Creative Commons Attribution (CC BY) license. (b) Lensless active transmission-mode imaging systems. From Han *et al.*, IEEE J. Solid-State Circuits **48**(10), 2296–2308 (2013). Copyright 2013 Author(s), licensed under a Creative Commons Attribution (CC BY) license.

CMOS has already been reported.[34] Additionally, the demonstration of a CMOS source with an output power of ~ -3 dBm at 700 GHz[17] along with the availability of 820-GHz CMOS detectors with a mean NEP of 36 pW/$\sqrt{\text{Hz}}$ also indicates that a full CMOS active transmission-mode imaging system is possible at 700 GHz and higher.

Lastly, the lensless operation[11] illustrated in Fig. 3(b) is also possible to simplify short-range imaging systems and to make them more compact and affordable.

IV. ACTIVE REFLECTION-MODE IMAGING

The more challenging and also one of the most compelling imaging modes for the submillimeter-wave community has been active reflection-mode imaging. The applications span imaging of targets at ∼1 cm or less for handheld uses to potentially targets many km's away for uses in airplanes and other fast-traveling systems. For example, imaging of cracks and voids in materials, imaging through a wall of wires and pipes, imaging through a package would require systems that can support a range of
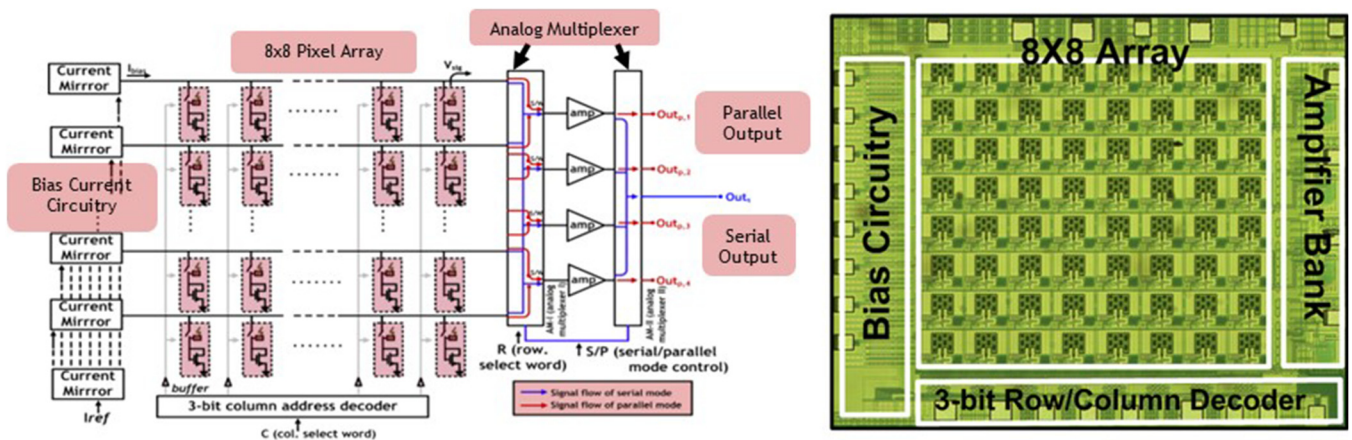

FIG. 4. 8 × 8 array of 820-GHz diode-connected NMOS transistor detectors incorporating an on-chip patch antenna with an on-chip bank of low noise amplifiers. The detectors can be individually accessed. From Kim *et al.*, IEEE Trans. Terahertz Sci. Technol. **6**(2), 306–317 (2016). Copyright 2016, Author(s), licensed under a Creative Commons Attribution (CC BY) license.

~1–30 cm. The maximum range of systems for the detection of hidden objects carried by people should be ~10 m, while that of systems for imaging through smoke and fire by emergency responders should be ~30–50 m. For use as a high angular resolution forward-looking radar imaging system in an automobile that can work in visually impaired situations, the range should be ~200 m, while use in an airplane would require the range to be many km's. Because of a wide bandwidth that can be used, this mode of imaging can also support a fine depth resolution.[56–59]

Despite the potential for a wide range of applications, the progress toward development and demonstration of affordable systems that have the potential for broad deployment has been slow. A 675-GHz imaging radar using a dual-folded reflector (1-m-diameter) with an angular resolution of 0.03° was demonstrated using a single transceiver fabricated in a III-V technology in combination with a mechanically rotating sub-reflector for increasing the field of view.[60] It was also demonstrated that the frame rate of such imaging systems can be increased by using an 1×8 focal plane array (FPA) of transceivers fabricated once again in III–V technologies with horn antennas[61] spaced by 12 mm. These systems are costly and consume high DC power, which limit their broad deployment. However, the recent demonstrations of 270 and 430-GHz CMOS concurrent transceiver pixels[44,45,62,63] that occupy an area of ~$(\lambda/2)^2$ and can be used to form large arrays are opening a path to overcome these limitations. This section discusses reflection-mode imaging using concurrent transceiver pixels for ranges between ~1 and ~200 m as well as for short ranges (~10 to ~200 mm without using an external lens or reflector). This section also presents the state of art for high depth resolution imaging using CMOS circuits.

A. Radar imaging using concurrent transceiver pixels

A concurrent pixel integrates a transmitter, a receiver, modulation circuits, and an on-chip antenna.[44,45,63] Figure 5(a) shows a circuit schematic of a 430-GHz concurrent transceiver radar pixels and a die photograph. A Colpitts oscillator operates at ~143.3 GHz and its third harmonic signal at 430 GHz is radiated through a differential patch antenna. The third harmonic signal is also used as a local oscillator signal to down convert the signal picked up by the antenna using an anti-parallel diode-connected NMOS transistor (DCNMOST) pair mixer to an intermediate frequency near 360 MHz. The pixel area is $374 \times 380\,\mu m^2$ or ~$\lambda/2 \times \lambda/2$. The pixel array shown in Fig. 5(b) is fabricated in 65-nm CMOS, and FSK modulated. The peak EIRP (Effective Isotropic Radiated Power) of array at 431.6 GHz is −4 dBm. The minimum DSB NF of a pixel is 38.5 dB at 431 GHz. Each pixel consumes around 29 mW of DC power. Using an 1×3 array of 430-GHz concurrent transceiver radar pixels and an external 6-cm diameter Cassegrain reflector in combination [Fig. 5(b)], images of a $6 \times 6\text{-cm}^2$ target 3-m away are formed through fog with an angular resolution of ~0.7° (Refs. 45 and 64) (Fig. 6). The sub-reflector diameter is 2.4 cm and the focal length of the main reflector is 3 cm. With a 15-cm diameter reflector, it should be possible to achieve an angular resolution less than 0.3°. Both images with and without fog in Fig. 6 clearly show the target (printed circuit board). The dynamic range of images in both cases is essentially the same

and over 30 dB when the measurement resolution bandwidth is 100 Hz. These *SNRs* indicate that the module can be used to image objects at larger stand-off distances.

Table I shows the link analysis for the 430-GHz concurrent transceiver[45] with a 15-cm diameter Cassegrain reflector at a range of 100 m. It includes 10-dB atmospheric loss.[65] The expected angular resolution is ~0.3° and scan step is 0.1°. For a Field of View (FoV) of 120° × 50°, the system generates radar images with ~600 000 pixels. To support a frame rate of 32/s, each pixel can have an integration time (1/32/600 000) of 52 ns. In order to increase the integration time to 1 μs or to reduce the noise bandwidth to ~1 MHz, 20 pixels can be activated simultaneously. This increases the power consumption of the focal plane array from ~30 to ~600 mW. Even with this, the SNR using the existing 430-GHz pixel is −16.5 dB, which is unacceptably low. The output power and noise figure of pixels must be improved.

The lowest double sideband noise figure reported for a CMOS down converter operating at 420 GHz[38] is ~14 dB. The highest output power from an anharmonic oscillator with an output around 400 GHz is ~−5 dBm.[66] Of course, these circuits occupy a larger area than $\lambda/2 \times \lambda/2$. However, if such performance can be incorporated into $\lambda/2 \times \lambda/2$ pixels, then the *SNR* can be greatly improved and may even allow increasing the range to 200 m. Such performance if realized, then will provide an alternative to LIDARs with an overlapping angular-resolution capability for automotive forward-looking imaging and ranging applications, which is lower cost and power consumption, and more importantly, can operate in visually impaired situations. Table I also suggests that if the receiver noise figure is reduced to 20 dB and the transmitter power is increased to −13 dBm, the *SNR* for imaging a target 100-m away can be increased to ~8.5 dB (in parentheses). Lastly, the 20 simultaneously activated transmit and receive pixels can be chosen to form subarrays such as 4×5 to further improve the SNR.[45]

The current commercial CMOS millimeter-wave radars and imaging systems employ phased arrays[48,49] and MIMO (Multiple Input Multiple Output) imaging.[50,67] To provide the two-way (transmission and reception) 106-dB passive gain of reflector in Table I using a phased array formed with the same concurrent pixels, the number of pixels, N in the array must be more than 3400 ($N^3 = 10^{10.6}$) instead of a single transmitter and a single receiver collocated in pixels. The power consumption of such an array is prohibitive and clearly illustrates the benefit of using reflectors with a high passive gain. To fully populate an area with a 15-cm diameter to support the 0.3° angular resolution, ~ 1 104 00 $400 \times 400\,\mu m$ pixels are needed. Such a phased array will provide a two-way gain of $10\log((110\,400)^3)$ ~150 dB. The transmitted power and sensitivity of the pixels in the array can be relaxed utilizing the extra 44 dB (150–106) gain. Despite this, the power consumption and complexity of implementing such a large array make this approach not practical for applications in which cost and form factor are limited.

The use of multiple input multiple output (MIMO) imaging[68,69] can reduce the combined number of transmitters and receivers to 2 x $(110\,400)^{0.4}$ ~660. However, because this number is substantially lower than 3400 needed for the two-way 106-dB gain, the SNR for a given integration time at the MIMO imaging system output will be $(3400/330)^3 = 1093$x lower than that of the system
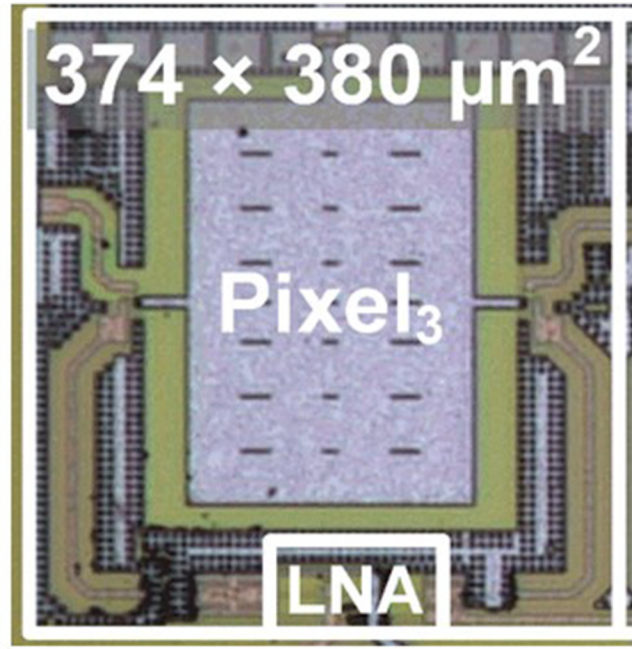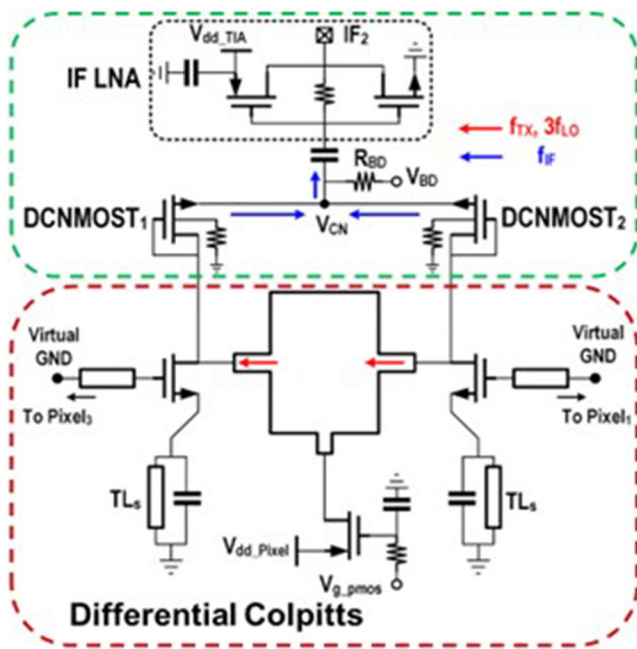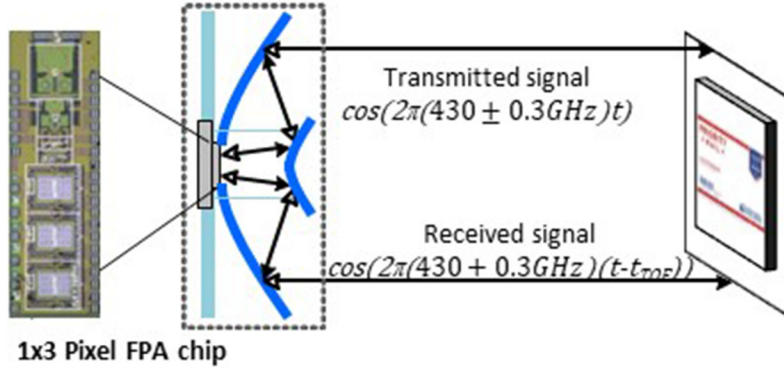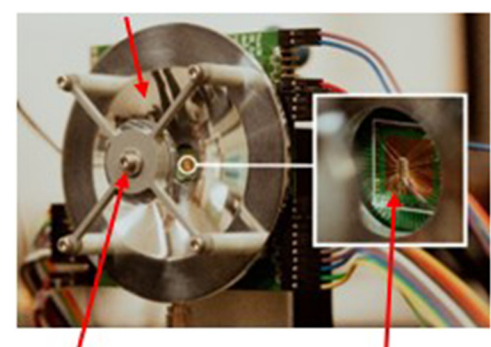
FIG. 5. (a) Circuit schematic and photograph of concurrent transceiver pixel integrating a transmitter, receiver, on-chip patch antenna, and injection locking circuit for stabilization of operating frequency.[64] (b) An 1 × 3 pixel array integrated with a 6-cm diameter Cassegrain reflector to form a reflection mode imager.[45,64] The sub-reflector diameter is 2.4 cm and the focal length of the main reflector is 3 cm.

using a 15-cm diameter Cassegrain reflector. Since MIMO imaging systems acquire return signals from the entire field of view in one shot, the integration time can potentially be increased by 1000X to 1 ms from 1 μs without affecting the frame rate of ~32/s to match the SNR of the system using a 15-cm diameter reflector. As mentioned, to provide a FoV of 120° × 50°, the system needs ~600 000 pixels. This means the MIMO system needs to have the total combined number of transmitters and receivers of ~$6 \times 2 \times (110\,400)^{0.5}$

~ 4000, though only 660 of them are activated at a given moment. Once again, the power consumption of such systems including that for the ~330 transmitters and ~330 receivers, and the backend computational resources to process the MIMO signals from ~330 receivers that pickup the signals from the 330 transmitters will be prohibitive for cost and size limited applications. Because of these, for the 100–200-m applications that need to be compact and affordable, the use of external optics for passive gain is compelling.
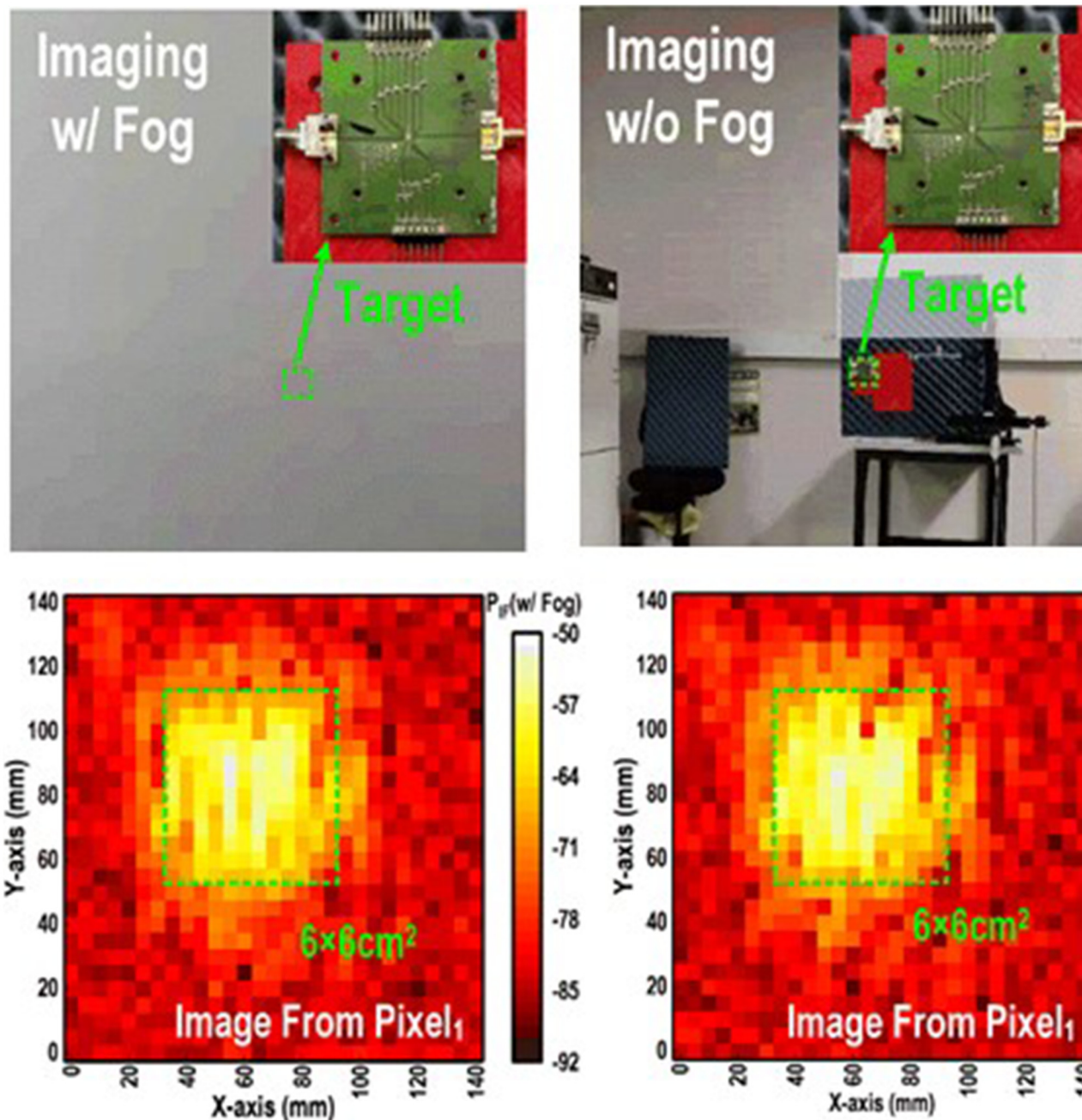
FIG. 6. Images formed of a $6 \times 6 \text{ cm}^2$ PCB 3-m away with and without fog[45,64] using the 430-GHz imaging module shown in Fig. 5. There is no significant difference between the images. Both images clearly show the PCB and the dynamic ranges in both cases are over 30 dB (resolution bandwidth = 100 Hz).

A problem with using optics such as a lens or a reflector is a limited field of view. A focal plane array that can cover a field of view of ~10° can be used with a reflector without significantly degrading the reflector performance. This, however, is still too small compared to the FoV target of $120° \times 50°$. Mechanical scanning is a straightforward approach to overcome this limitation. However, it increases system volume, cost, and power consumption as well as reliability challenges. A way to bypass these is using

TABLE I. Link margin analysis for reflection mode imaging at 100-m range using a 430-GHz concurrent transceiver pixel[45] and an external reflector with a diameter of 15 cm. (): Improvement opportunities based on the published data.

Imaging at 100 m (1 TX and 1 RX with 15-cm diameter reflector)			
Frequency	400 GHz	R^{-4} @ 100 m	-80 dB/m^4
$P_{transmitted}$	-18 (-13) dBm	Atmos. loss	10 dB
Antenna gain (G^2)	3.5 + 3.5 dB	$P_{received}$	-90.5 (-85.5) dBm
Reflector diameter	15 cm	kT	-174 dBm/Hz
Aperture efficiency	-3 dB, -3 dB	Noise figure	40 (20) dB
Reflector gain	56 + 56 dB	B (bandwidth)	60 dB-Hz
Radar cross section (σ)	0 dB-m^2	Noise floor	-74 (-94) dBm
$\lambda^2/(4\pi)^3$ @400 GHz	-95.5 dB-m^2	SNR	-16.5 (8.5) dB
Field of view	120° × 50°	Number of pixels	600 000
Scan step	0.1°	Frame rate	32/s
$t_{integration}$ @ 20 pixels on	1.04 μs	Angular resolution	0.3°

electronically steerable reflect arrays[70,71] to form external optics. Besides increasing the output power and improving the sensitivity of pixels, realizing affordable and power efficient steerable reflect arrays is a key technical challenge to enable broad utilization of submillimeter-wave imaging.

B. Short-range external opticless reflection-mode imaging with concurrent pixels

A submillimeter-wave/terahertz imaging system that captured the imagination of the public is the implementation which can be placed in the back of a smartphone that allows imaging through packages and envelops for identification of contents, and imaging of wires, wooden beams and pipes behind walls, markers that cannot be seen by eyes for authentication, sub-surface cracks, and others. Such systems cannot employ external optics/reflectors because of the thickness requirement of smartphones or other portable devices. The most troubling concern for making such capabilities widely available is protecting privacy. These are essentially the same technology as that is used to detect hidden objects in the security lines at airports. For inclusion in portable devices that are widely used, the capability must be limited to ensure privacy. More specifically, the range should be limited to less than ~20 cm.

Figure 7(a) shows a conceptual illustration of such reflection mode imaging systems which was first discussed in the presentation of a 2012 paper[35] that reported an incoherent 280-GHz Schottky diode detector focal plane array fabricated in CMOS. The imaging elements can be manually scanned over targets to create images. Recently, a reflection mode imager using a 60-GHz 8 × 8 cm^2 radar module including 20 transmitters, 20 receivers, and 20 TX and 20 RX antennas distributed over a length of ~16 cm along the two edges of the module[67] has become commercially available. This module is integrated into a device that can be attached onto the backside of a smartphone. The device footprint is approximately the same as that of a smartphone while its height is ~1.5X of that of a smartphone, which is bulky. Its angular resolution limit is 6.7°.
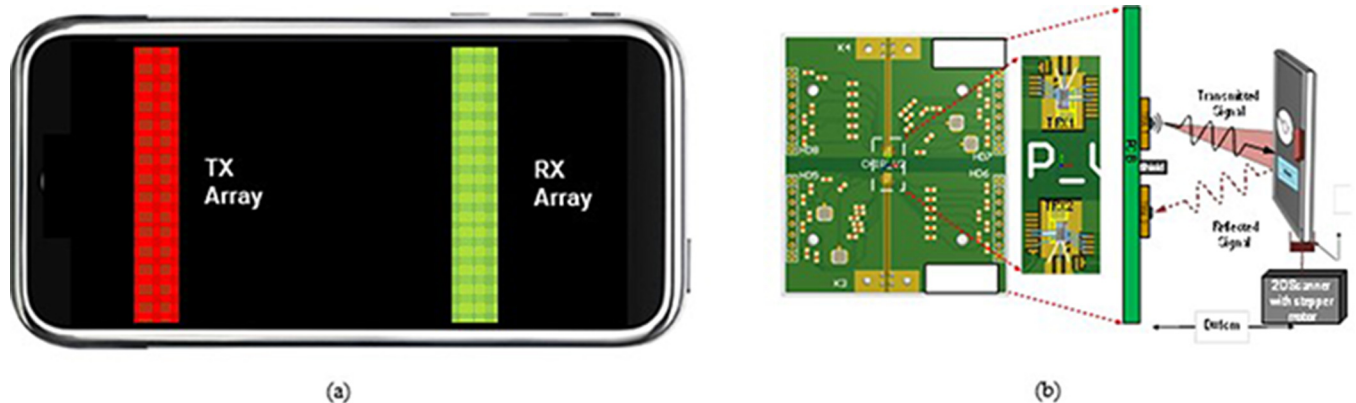

FIG. 7. (a) Conceptual diagram for reflection mode imager on the back of a smartphone. (b) Operation principle of reflection-mode 275-GHz imager without using external optics.[75]
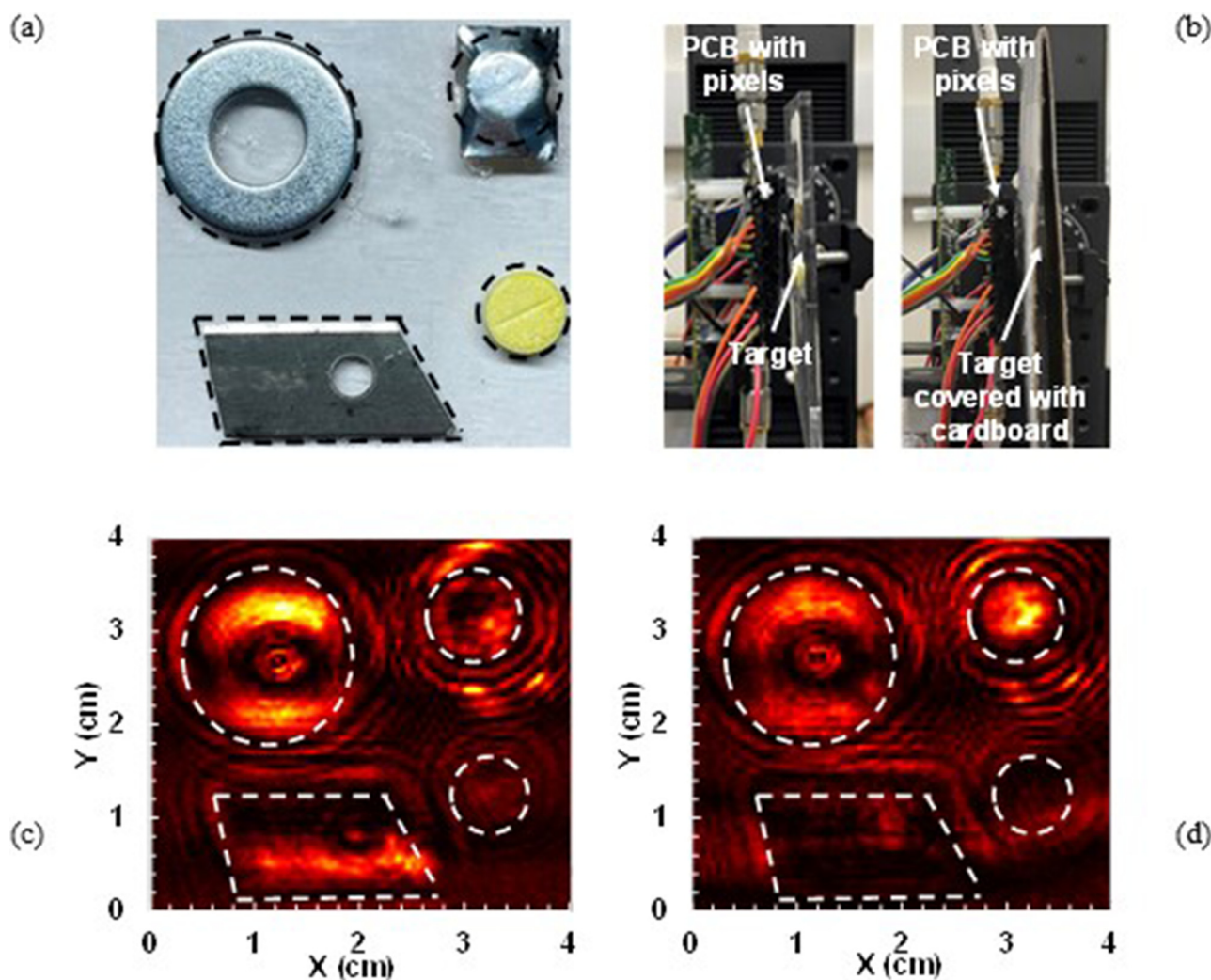
FIG. 8. (a) Target with washer, blade, and pills. (b) Side views of imaging setup with and without a cardboard cover, (c) 275-GHz image of the target in (a) without and (d) with a cardboard cover. From Byreddy *et al.*, IEEE Sensor Lett. **7**(2), 3500204 (2023). Copyright 2023 Author(s), licensed under a Creative Commons Attribution (CC BY) license.

Additionally, a 60-GHz radar module (Soli[72]) for gesture recognition has also been incorporated in smartphones. Its footprint is $\sim 10 \times 10$ mm^2.[72]

For systems operating at 300 GHz, an aperture with a diameter of 10 mm or $\sim 10\lambda$ which can be easily incorporated into a smartphone should be able to support an angular resolution of $\sim 7°$. To demonstrate such 300-GHz imaging systems fabricated in CMOS, the noise floor of detector/receiver had to be improved using a coherent detector by multiple orders of magnitude over that of the Schottky diode detectors,[35] and transmitters with a sufficient output power level had to be realized. Furthermore, the area of coherent receivers had to be reduced to $\lambda/2 \times \lambda/2$ or $\sim 500 \times 500$ μm^2 for operation near 300 GHz,[43,73,74] so that a group of the receivers/pixels can be used to form a focal plane array

(FPA). The improvement of transmitter output power[19–21] and realization of coherent receivers/pixels with improved sensitivities that occupy an area of nearly $\lambda/2 \times \lambda/2$[43–45,62,63,73,74] over the past 10 years have led to the demonstration of 275-GHz reflection mode imaging without using an external optics. This demonstration also suggests the feasibility of incorporating such capabilities on the backside of a smartphone. Figure 7(b) shows a printed circuit board and configuration of pixels used for the reflection-mode imaging demonstration without using external optics.[75]

The demonstration utilized two integrated circuits incorporating a 275-GHz concurrent transceiver pixel utilizing an on-chip patch antenna and injection locking circuit to stabilize the oscillation frequency of the pixel. The first IC operates as a receiver while the other functions as a transmitter. The concurrent pixel delivers an effective

TABLE II. Link margin analyses for reflection mode imaging without external optics of targets 200-mm away. (): Improvement opportunities based on the published data.

Short-range imaging at a range of 200 mm (20 TX pixels and 1 RX pixel)			
Frequency	300 GHz	Noise figure	51 (20) dB
$P_{transmitted}$	−21 (−13) + 13 dBm	B (bandwidth)	35 dB-Hz
Antenna gain (G^2)	15 + 2 dB	Noise floor	−88 (−119) dBm
Rad. cross section (σ)	5 dB-mm^2	R^{-4} @ 200 mm	−92 dB/mm^4
$\lambda^2/(4\pi)^3$ @300 GHz	−33 dB-mm^2	$P_{received}$	−111 (−103) dBm
kT	−174 dBm/Hz	SNR	−23 (16) dB

isotropic radiated power of −18.9 dBm,[75] exhibits a double sideband (DSB) noise figure of ∼51 dB, and occupies an area of 0.45×0.49 mm^2 which is less than $\lambda/2 \times \lambda/2$ at 300 GHz. This printed circuit board is utilized to demonstrate reflection-mode imaging of objects ∼10-mm away without employing external optics.

A target shown in Fig. 8(a) includes a washer, a blade, and a pill with and without a wrapper. Figure 8(b) shows the setup including the target with and without an ∼1-mm thick cardboard cover. The target is located 10-mm away from the PCB and is scanned over an area of 40×40 mm^2 with a step of 0.5 mm. The integration time was ∼1 ms. Figures 8(c) and 8(d) show the reflection mode images without and with the cardboard cover, respectively. The dynamic range of the images is ∼30 dB. Covering the target with the cardboard lowers the received power by ∼4 dB. The hole in the blade has a diameter of 4 mm and is clearly seen in the images, indicating that the resolution limit is less than this.[75] As a matter of fact, an imaging experiment with a resolution target indicates that the resolution limit is ∼2 mm.

Figure 7(a) more specifically shows a conceptual illustration of a 300-GHz imager incorporated on the backside of a smartphone using a transmitter and a receiver array occupying an area of ∼50×10 mm^2, respectively. These arrays can be used to manually scan and form SAR (Synthetic Aperture Radar)[50] images that have much better resolution than that limited by the transmitter and receiver array area. In an area of 50×10 mm^2, ∼ 2 000 $\lambda/2 \times \lambda/2$ pixels can be placed. To support a frame rate of 32/s, the integration time for each pixel must be less than 15.6 μs (1/32/2000). If 20 pixels are activated simultaneously, then the integration time can be increased to ∼300 μs and the noise bandwidth can be reduced to ∼3 kHz.

Table II shows the link analysis at a range of 200 mm for corporal subarrays of 20 transmitters and 20 receivers on a $\lambda/2$ grid over an area of ∼2×2.5 mm^2 (4×5 pixels). These subarrays can be formed using the pixels in the 50×10 mm^2 transmitter and receiver arrays. The radar cross section is assumed to be 3 mm^2, which is small for a target 200-mm away. Utilizing 20 transmitters increases the power incident to a receiver by 26 dB. The outputs of 20 receivers are not combined with that of other receivers in order to support the frame rate target while increasing the integration time. The *SNR* is −23 dB, which is too low. Once again, the pixel

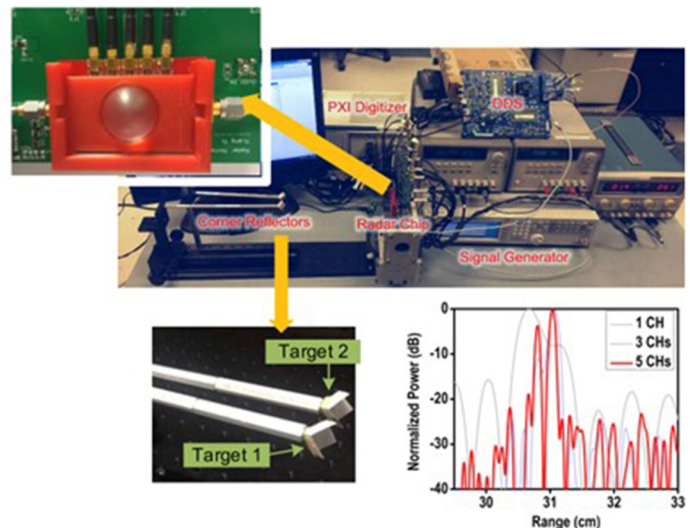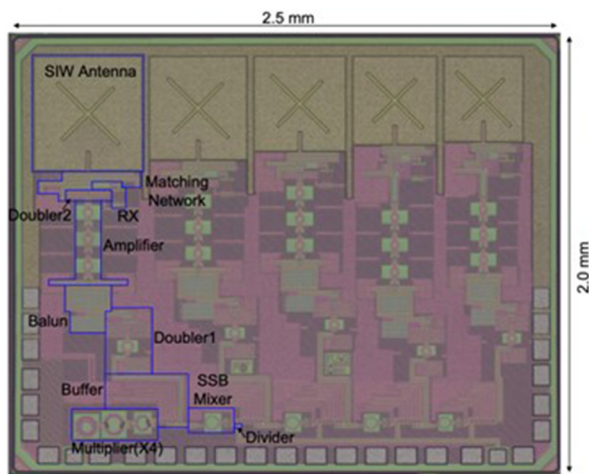**FIG. 9.** Die photograph of 220–320 GHz FMWC radar IC fabricated in 65-nm CMOS and the measurement setup including two corner reflectors with a depth difference of 2.0 mm. The two objects are well resolved after stitching the output data of five radar channels. From Yi *et al.*, IEEE J. Solid-State Circuits **56**(2), 327–339 (2021). Copyright 2021 Author(s), licensed under a Creative Commons Attribution (CC BY) license.

TABLE III. Capabilities that can be supported by the present-day CMOS imaging circuits as well as those requiring further research efforts (Trans.: transmission mode, Refl.: reflection mode).

Imaging mode	Frequency (GHz)	Range	Aperture diameter	Resolution (angular) (deg)	Resolution (distance)	Depth resolution
Capabilities that can be supported by the existing CMOS imaging circuits						
Trans. exter. optics	280	200 mm	200 mm		2.5 mm	
Trans. lensless	280	20 mm	0.5 mm	60	2 mm	
Trans. lensless	430	20 mm	0.4 mm	60	~1.4 mm	
Refl. exter. reflector	430	30 m	150 mm	0.3	0.15 m	150 mm
Refl. lensless	274	10 mm	0.5 mm	60	~2 mm	
Refl. lensless	430	10 mm	0.4 mm	60	~1.4 mm	
Refl. 3D	220–320	200 mm	25.4 mm			1.5 mm
Capabilities that require further CMOS imaging circuits and other research						
Refl. exter. reflector	400	200 m	150 mm	0.3	1.0 m	15 mm
Refl. exter. reflector	850	100 m	150 mm	0.15	0.25 m	15 mm
Refl. lensless	300	200 mm	10 mm		~2 mm	15 mm
Refl. lensless	400	200 mm	8 mm		~1.4 mm	15 mm

performance must be improved. Table II also suggests that if the receiver noise figure is reduced to 20 dB and the transmitter power is increased to −13 dBm, the *SNR* for imaging a target 200-mm away without the aid of external optics can be increased to 16 dB (in parentheses) and the imaging in this situation can be made feasible.

The lowest double sideband noise figure reported for a CMOS down converter operating near 300 GHz[37,76] is ~11–14 dB. The highest output power from a single chain 300-GHz CMOS transmitter is ~−6 dBm.[77] Of course, these circuits once again occupy a larger area than $\lambda/2 \times \lambda/2$. If such performance can be incorporated into $\lambda/2 \times \lambda/2$ pixels, then an *SNR* greater than 30 dB can be provided at a range to target of 200 mm. Given these, the −13-dBm transmitted power and 20-dB noise figure targets for a $\lambda/2 \times \lambda/2$ pixel in Table II certainly do not appear to be unrealistic. These suggest that there should be paths to realize a lensless system using 300-GHz CMOS pixels that can support a range of 200 mm.

Lastly, isolation of the signal from a transmitter that directly couples to the receiver pixels without reflection from targets is another challenge for imaging at ranges of 100–200 mm. The reflected signals from targets picked up by the receiver pixels must be greater than the sum of required SNR (dB) and the directly coupled signal (dBm). Optimization of the separation between transmitter and receiver pixels, inclusion of a conductive wall, and cancellation of direct coupling can be utilized to reduce their impact. Realizing pixels with the adequate performance at a range of 200 mm and systems with sufficient suppression of direct coupling are the present challenges for making inclusion of reflection-mode submillimeter-wave imaging in a smartphone possible.

C. Broadband imaging with a fine depth resolution

Another exciting opportunity within the submillimeter-wave frequency range is 3D imaging with a high depth resolution taking advantage of the availability of wide frequency bands. In the FMCW (Frequency Modulated Continuous Wave) radar mode, the ranging resolution is inversely proportional to the spectral scanning bandwidth. This in combination with an inverse synthetic aperture radar (ISAR) technique[56] would make rapid and mm-depth resolution 3D imaging possible. Prior single-transceiver works have achieved a bandwidth up to ~60 GHz.[56,57] However, there is a tradeoff in these circuits between the bandwidth and output power (TX) and between the bandwidth and sensitivity (RX). The broadband radar transceivers, therefore, all exhibit large performance degradation at the two edges of the band. A multi-transceiver architecture that leverages the high integration capability of CMOS technologies allows for a seamless band coverage from 220 to 320 GHz[58] using five 20-GHz bandwidth transceivers and substrate integrated waveguide (SIW) antennas tuned at five different center frequencies. Figure 9 shows a die photograph of the IC[69] fabricated in 65-nm CMOS and the measurement setup including two corner reflectors with a depth difference of 2.0 mm that were used to demonstrate the ~1.5-mm depth resolution. A 2-cm diameter Teflon lens was mounted on a radar IC to increase the range. The depth resolution is defined as the minimum distance between two resolvable objects placed in the longitudinal direction. In many high-lateral resolution imaging scenarios where the beam is well focused, it can be assumed that an echo is created by a single object/surface. Under this assumption, much higher depth resolution can be achieved by examining the phase of the echo. Exploiting this, a depth resolution of 54 μm is demonstrated using a 250-GHz FMCW radar.[59]

V. CONCLUSIONS

The performance of CMOS sources/transmitters and detectors/receivers operating at the submillimeter electromagnetic wave frequencies have sufficiently improved for use in active transmission and reflection-mode imaging applications that have the potential for broad deployment and utilization. Table III summarizes the

capabilities that can be supported by the present-day CMOS imaging circuits as well as those requiring further research efforts. The CMOS circuit and system performances are suitable for use in commercially available systems that have a wide range of transmission-mode imaging applications. For centimeters reflection-mode imaging, applications with a range of a few cms without using external optics and with a range of less than ∼30 m using external optics can be supported using the state-of-the-art CMOS circuits. Improving the performance of CMOS circuits to increase the range to 200 mm and to higher than 200 m for applications without and with external optics, respectively, is the current research challenge.

The electronically steerable reflector technology is a key that can drastically improve the performance and power efficiency of medium to short-range submillimeter-wave imaging systems. There are propagation windows at 650 and 850 GHz. Increasing the operating frequency from 430 to 850 GHz to improve the angular resolution by 2X at a given form factor (∼0.15° for a reflector diameter of 15 cm) will increase the two-way reflector gain by 12 dB ($\sim f^4$), while decreasing the transmitter output power by ∼10 dB (−10 dB/octave) and increasing the receiver noise figure by ∼5 dB (15 dB/decade). The net degradation to the SNR is 3 dB, which can be tolerated. However, at 850 GHz and a range of 200 m, the atmospheric loss in 20-mm/h rain is 40 dB instead of 20 dB at 400 GHz.[65] In addition, the reflector loss is expected to increase due to the increase in loss of the phase-tuning elements used in steerable reflectors with frequency. An angular resolution of 0.15° will make the submillimeter-wave imaging competitive to the LIDAR performance. Improvements to the circuit techniques and devices are needed. The use of the BiCMOS technologies that provide SiGe HBTs with a f_{max} of 600–700 GHz[78] will enable earlier demonstration of such systems.

AUTHOR DECLARATIONS

Conflict of Interest

The authors have no conflicts to disclose.

Author Contributions

Kenneth K. O: Conceptualization (lead); Data curation (equal); Formal analysis (equal); Funding acquisition (equal); Investigation (equal); Methodology (equal); Project administration (equal); Resources (equal);Validation (equal); Visualization (equal); Writing – original draft (lead); Writing – review & editing (equal).**Wooyeol Choi:** Conceptualization (equal); Data curation (equal); Formal analysis (equal); Funding acquisition (equal); Investigation (equal); Methodology (equal); Project administration (equal); Resources (equal); Supervision (equal); Validation (equal); Visualization (equal); Writing – original draft (equal); Writing – review & editing (equal). **Ruonan Han:** Conceptualization (equal); Data curation (equal); Formal analysis (equal); Funding acquisition (equal); Investigation (equal); Methodology (equal); Project administration (equal); Resources (equal); Supervision (equal); Validation (equal); Visualization (equal); Writing – original draft (equal); Writing – review & editing (equal).

DATA AVAILABILITY

The data that support the findings of this study are available within the article.

REFERENCES

[1]B. B. Hu and M. C. Nuss, "Imaging with terahertz waves," Opt. Lett. **20**(16), 1716–1719 (1995).

[2]M. Tonouchi, "Cutting-edge terahertz technology," Nat. Photonics **1**, 97–105 (2007).

[3]D. M. Mittleman, "Twenty years of terahertz imaging [invited]," Opt. Express **26**, 9417–9431 (2018).

[4]F. Friederich, W.von Spiegel, M. Bauer, M. Fanzhen, M. D. Thomson, S. Boppel, A. Lisauskas, B. Hils, V. Krozer, A. Keil, T. Loffler, R. Henneberger, A. K. Huhn, G. Spickermann, P. H. Bolivar, and H. G. Roskos, "THz active imaging systems with real-time capabilities," IEEE Trans. Terahertz Sci. Technol. **1**(1), 183–200 (2011).

[5]G. Valušis, A. Lisauskas, H. Yuan, W. Knap, and H. G. Roskos, "Roadmap of terahertz imaging 2021," Sensors **21**, 4092 (2021).

[6]D. Huang, T. R. LaRocca, L. Samoska, A. Fung, and M.-C. F. Chang, "324 GHz CMOS frequency generator using linear superposition technique," in *IEEE ISSCC Digest of Technology Papers* (IEEE, 2008), pp. 476–477.

[7]E. Seok, C. Cao, D. Shim, D. J. Arenas, D. B. Tanner, C.-M. Hung, and K. K. O, "410-GHz CMOS push-push oscillator with a patch antenna," in *2008 International Solid-State Circuits Conference*, San Francisco, CA (IEEE, 2008), pp. 472–473.

[8]U. R. Pfeiffer and E. Öjefors, "A 600 GHz CMOS focal-plane array for terahertz imaging applications," in *Proceedings of European Solid-State Circuits Conference* (IEEE, 2008), pp. 110–114.

[9]R. L. Schmid, A. Ulusoy, S. Zeinolabedinzadeh, and J. D. Cressler, "A comparison of the degradation in RF performance Due to device interconnects in advanced SiGe HBT and CMOS technologies," IEEE Trans. Electron Devices **62**(6), 1803–1810 (2015).

[10]Q. Zhong, W. Choi, D.-Y. Kim, Z. Ahmad, R. Xu, Y. Zhang, R. Han, S. Kshattry, N. Sharma, Z.-Y. Chen, D. Shim, S. Sankaran, E.-Y. Seok, C. Mao, F. C. De Lucia, J. P. McMillan, C. F. Neese, I. Kim, I. Momson, P. Yelleswarapu, S. Dong, B. Pouya, P. Byreddy, Z. Chen, Y. Zhu, S. Ghosh, T. Dinh, F. Jalalibidgoli, J. Newman, and K. K. O, in *2018 IEEE Custom Integrated Circuits Conference, Paper 13-5, San Diego, CA* (IEEE, 2018).

[11]R. Han, Y. Zhang, Y. Kim, D.-Y. Kim, H. Shichijo, E. Afshari, and K. K. O, "Active THz imaging using SBD's in CMOS: Array and 860-GHz pixel," IEEE J. Solid-State Circuits **48**(10), 2296–2308 (2013).

[12]W. Steyaert and P. Reynaert, "A 0.54 THz signal generator in 40 nm bulk CMOS with 22 GHz tuning range and integrated planar antenna," IEEE J. Solid-State Circuits **49**(7), 1617–1626 (2014).

[13]Z. Chen, Z.-Y. Chen, W. Choi, and K. K. O, "610-GHz fourth harmonic signal reactively generated in a CMOS voltage controlled oscillator using differentially pumped varactors," IEEE Solid-State Circuits Lett. **3**, 46–49 (2020).

[14]Y. M. Tousi, O. Momeni, and E. Afshari, "A novel CMOS high-power terahertz VCO based on coupled oscillators: Theory and implementation," IEEE J. Solid-State Circuits **47**(12), 3032–3042 (2012).

[15]K. Guo and P. Reynaert, "29.2 A 0.59 THz beam-steerable coherent radiator array with 1 mW radiated power and 24.1dBm EIRP in 40 nm CMOS," in *2020 IEEE International Solid- State Circuits Conference - (ISSCC)* (IEEE, 2020), pp. 442–444. doi:10.1109/ISSCC19947.2020.9063139.

[16]Z. Ahmad, M. Lee, and K. K. O, "A 1.4THz, -13dBm EIRP multiplier chain in 65-nm CMOS using symmetric & asymmetric-CV varactors," in *2016 IEEE International Solid State Circuits Conference, San Francisco, CA* (IEEE, 2016), pp. 350–351.

[17]L. Gao and C. H. Chan, "A 0.68–0.72-THz 2-D scalable radiator array with −3-dBm radiated power and 27.3-dBm EIRP in 65-nm CMOS," IEEE J. Solid-State Circuits **57**(10), 3114–3124 (2022).

[18]O. Momeni and E. Afshari, "High power terahertz and millimeter-wave oscillator design: A systematic approach," IEEE J. Solid-State Circuits **46**(3), 583–597 (2011).

[19]S. Jameson and E. Socher, "A 0.3 THz radiating active X27 frequency multiplier chain with 1 mW radiated power in CMOS 65-nm," IEEE Trans. Terahertz Sci. Technol. **5**(4), 645–648 (2015).

[20]Z. Ahmad, I. Kim, and K. K. O, "0.39-0.45THz symmetric MOS-varactor frequency tripler in 65-nm CMOS," in *IEEE RFIC Symposium, Pheonix, AZ* (IEEE, 2015).

[21]R. Han and E. Afshari, "A high-power broadband passive terahertz frequency doubler in CMOS," IEEE Trans. Microw. Theory Tech. **61**(3), 1150–1160 (2013).

[22]C. Cao, E. Seok, and K. K. O, "192-GHz push-push VCO in 0.13-μm CMOS," Electron. Lett. **42**(4), 208–209 (2006).

[23]D. Parveg, D. Karaca, M. Varonen, A. Vahdati, and K. A. I. Halonen, "Demonstration of a 0.325-THz CMOS amplifier," in *2016 Global Symposium on Millimeter Waves (GSMM) & ESA Workshop on Millimeter-Wave Technology and Applications* (IEEE, 2016), pp. 1–3.

[24]B. Yun, D.-W. Park, C.-G. Choi, H.-J. Song, and S.-G. Lee, "280.2/309.2 GHz, 18.2/9.3 dB gain, 1.48/1.4 dB gain-per-mW, 3-stage amplifiers in 65 nm CMOS adopting double-embedded-gmax-core," in *2022 IEEE Radio Frequency Integrated Circuits Symposium (RFIC)* (IEEE, 2022), pp. 91–94.

[25]W. Knap, F. Teppe, Y. Meziani, N. Dyakonova, J. Lusakowski, F. Boeuf, T. Skotnicki, D. Maude, S. Rumyantsev, and M. S. Shur, "Plasma wave detection of sub-terahertz and terahertz radiation by silicon field-effect transistors," Appl. Phys. Lett. **85**(4), 675–677 (2004).

[26]D.-Y. Kim, S. Park, R. Han, and K. K. O, "Design and demonstration of 820-GHz array using diode-connected NMOS transistors in 130-nm CMOS for active imaging," IEEE Trans. Terahertz Sci. Technol. **6**(2), 306–317 (2016).

[27]Z. Ahmad and K. K. O, "THz detection using p+/n-well diodes fabricated in 45-nm CMOS," IEEE Electron Device Lett. **37**(7), 823–826 (2016).

[28]E. Seok, C. Cao, S. Sankaran, and K. K. O, "A mm-wave Schottky diode detector in 130-nm CMOS," in *Symposium on VLSI Circuits, Honolulu, HI* (IEEE, 2006), pp. 178–179.

[29]S. Sankaran and K. K. O, "Schottky barrier diodes for millimeter wave and detection in a foundry CMOS process," IEEE Electron Device Lett. **26**(7), 492–494 (2005).

[30]A. Lisauskas, M. Bauer, S. Boppel, M. Mundt, B. Khamaisi, E. Socher, R. Venckevičius, L. Minkevičius, I. Kašalynas, G. Seliuta, G. Valušis, V. Krozer, and H. G. Roskos, "Exploration of terahertz imaging with silicon MOSFETs," J. Infrared, Millimeter, Terahertz Waves **35**(1), 63–80 (2014).

[31]Z. Ahmad, A. Lisauskas, H. G. Roskos, and K. K. O, "9.74-THz electronic Far-infrared detection using Schottky barrier diodes in CMOS," in *2014 International Electron Devices Meeting, Paper 4.4, San Francisco, CA* (IEEE, 2014).

[32]Z. Ahmad, A. Lisauskas, H. G. Roskos, and K. K. O, "Design and demonstration of antenna-coupled Schottky diodes in a foundry complementary metal-oxide semiconductor technology for electronic detection of Far-infrared radiation," J. Appl. Phys. **125**(19), 194501 (2019).

[33]Schuster, H. Videlier, A. Dupret, D. Coquillat, M. Sakowicz, J. Rostaing, M. Tchagaspanian, B. Giffard, and W. Knap, "A broadband THz imager in a low-cost CMOS technology," in *IEEE International Solid-State Circuits Conference (ISSCC) Digest of Technical Papers, San Francisco, CA* (IEEE, 2011).

[34]H. Sherry, J. Grzyb, Y. Zhao, R. A. Hadi, A. Cathelin, A. Kaiser, and U. Pfeiffer, "A 1 k-pixel CMOS camera chip for 25 fps real-time terahertz imaging applications," in *2012 IEEE International Solid-State Circuits Conference (ISSCC) Digest of Technical Papers* (IEEE, 2012), pp. 252–254.

[35]R. Han, Y. Zhang, Y. Kim, D.-Y. Kim, H. Shichijo, E. Afshari, and K. K. O, "280 GHz and 860 GHz image sensors using Schottky-barrier diodes in 0.13 μm digital CMOS," in *2012 International Solid-State Circuits Conference, San Francisco, CA* (IEEE, 2012), pp. 254–256.

[36]Q. Zhong, W.-Y. Choi, and K. K. O, "Terahertz even-order subharmonic mixer using symmetric MOS varactors," IEEE J. Solid-State Circuits **56**(2), 355–366 (2021).

[37]Q. Zhong, W. Choi, C. Miller, R. Henderson, and K. K. O, "A 210-to-305 GHz CMOS receiver for rotational spectroscopy," in *IEEE International Solid State Circuits Conference, San Francisco, CA* (IEEE, 2016), pp. 426–427.

[38]I. Momson, S. Lee, S. Dong, and K. K. O, "425-to-25-GHz CMOS-integrated downconverter," IEEE Solid-State Circuits Lett. **4**, 80–83 (2021).

[39]J. Zhou and X. Luo, "An 820-GHz down-converter with fourth subharmonic mixer in 40-nm CMOS technology," IEEE Microw. Wirel. Compon. Lett. **31**(10), 1146–1149 (2021).

[40]B. Khamaisi, S. Jameson, and E. Socher, "A 0.58–0.61THz single on-chip antenna transceiver based on active X30 lO chain on 65 nm CMOS," in *2016 11th European Microwave Integrated Circuits Conference (EuMIC)* (IEEE, 2016), pp. 97–100.

[41]U. R. Pfeiffer, E. Ojefors, A. Lisaukas, D. Glaab, and H. G. Roskos, "A CMOS focal-plane array for heterodyne terahertz imaging," in *2009 IEEE Radio Frequency Integrated Circuits Symposium* (IEEE, 2009), pp. 433–436.

[42]C. Jiang *et al.*, "A fully integrated 320 GHz coherent imaging transceiver in 130 nm SiGe BiCMOS," IEEE J. Solid-State Circuits **51**(11), 2596–2609 (2016).

[43]Z. Hu, C. Wang, and R. Han, "Heterodyne sensing CMOS array with high density and large scale: A 240-GHz, 32-unit receiver using a de-centralized architecture," in *2018 RFIC Symposium, RTU1B-4* (IEEE, 2018), pp. 252–255.

[44]W. Choi, P. R. Byreddy, Z.-Y. Chen, Z. Chen, A. J. Newman, and K. K. O, "450×580-μm^2 pixel incorporating TX and coherent RX in CMOS for mm-wave active imaging using a single reflector," Electron. Lett. **54**(16), 982–984 (2018).

[45]Y. Zhu, P. Byreddy, K. K. O, and W. Choi, "430-GHz CMOS concurrent transceiver pixel array for high angular resolution reflection-mode active imaging," in *IEEE International Solid-State Circuits Conference, San Francisco, CA* (IEEE, 2022).

[46]A. Tang and M.-C. F. Chang, "183-GHz 13.5 mW/pixel CMOS regenerative receiver for mm-wave imaging applications," in *2011 IEEE International Solid State Circuits Conference, San Francisco, CA* (IEEE, 2011), pp. 296–297.

[47]W. Choi, Z. Ahmad, A. Jha, J.-Y. Lee, I. Kim, and K. K. O, "410-GHz CMOS imager using a 4th Sub-harmonic mixer with effective NEP of 0.3 fW/Hz0.5 at 1-kHz noise bandwidth," in *2015 IEEE VLSI Symposium on Circuits, Kyoto, Japan* (IEEE, 2015), pp. C302–C303.

[48]B. P. Ginsburg *et al.*, "A multimode 76-to-81 GHz automotive radar transceiver with autonomous monitoring," in *IEEE International Solid-State Circuits Conference, San Francisco, CA* (IEEE, 2018), pp. 158–159.

[49]T. Arai *et al.*, "A 77-GHz 8RX3TX transceiver for 250-m long-range automotive radar in 40-nm CMOS technology," IEEE J. Solid-State Circuits **56**(5), 1332–1344 (2021).

[50]M. E. Yanik and M. Torlak, "Near-Field MIMO-SAR millimeter-wave imaging with sparsely sampled aperture data," IEEE Access **7**, 31801–31819 (2019).

[51]A. Visweswaran *et al.*, "A 145 GHz FMCW-radar transceiver in 28 nm CMOS," in *IEEE International Solid-State Circuits Conference, San Francisco, CA* (IEEE, 2019), pp. 168–169.

[52]A. V. Shchepetilnikov, P. A. Gusikhin, V. M. Muravev, B. D. Kaysin, G. E. Tsydynzhapov, A. A. Dremin, and I. V. Kukushkin, "Linear scanning system for THz imaging," Appl. Opt. **60**(33), 10448–10452 (2021).

[53]U. R. Pfeiffer, E. Öjefors, A. Lisaukas, D. Glaab, F. Voltolina, V. F. Nzogang, P. Bolivar, and H. Roskos, "A CMOS focal-plane array for terahertz imaging," in *Proceedings of the 33rd International Conference on Infrared, Millimeter, and Terahertz Waves, Pasadena, CA* (IEEE, 2008).

[54]A. Lisaukas, U. Pfeiffer, E. Öjefors, P. H. Bolívar, D. Glaab, and H. G. Roskos, "Rational design of high-responsivity detectors of terahertz radiation based on

distributed self-mixing in silicon field-effect transistors," J. Appl. Phys. **105**, 114511 (2009).

[55]N. Buadana, S. Jameson, and E. Socher, "A 280 GHz +9dBm TRP dense 2D multi port radiator in 65 nm CMOS," in *2018 IEEE Radio Frequency Integrated Circuits Symposium (RFIC)* (IEEE, 2018), pp. 248–251.

[56]A. Mostajeran *et al.*, "A high-resolution 220-GHz ultra-wideband fully integrated ISAR imaging system," IEEE Trans. Microw. Theory. Tech. **67**(1), 429–442 (2019).

[57]J. Grzyb, K. Statnikov, N. Sarmah, B. Heinemann, and U. R. Pfeiffer, "A 210–270-GHz circularly polarized FMCW radar with a single-lens-805 coupled SiGe HBT chip," IEEE Trans. Terahertz Sci. Technol. **6**(6), 771–783 (2016).

[58]X. Yi, C. Wang, J. Garajal, and R. Han, "A 220-to-320-GHz FMCW radar frontend in 65-nm CMOS using a frequency-comb architecture," IEEE J. Solid-State Circuits **56**(2), 327–339 (2021).

[59]S. M. Hossein Naghavi, S. Seyedabbaszadehesfahlani, F. Khoeini, A. Cathelin, and E. Afshari, "A 250 GHz autodyne FMCW radar in 55 nm BiCMOS with micrometer range resolution," in *Dig.: Tech. Pap. - IEEE International Solid-State Circuits Conference* (IEEE, 2021), Vol. 64, pp. 320–322.

[60]K. B. Cooper, R. J. Dengler, N. Llombart, B. Thomas, G. Chattopadhyay, and P. H. Siegel, "THz imaging radar for standoff personnel screening," IEEE Trans. Terahertz Sci. Technol. **1**(1), 169–182 (2011).

[61]K. B. Cooper, "Performance of a 340 GHz radar transceiver array for standoff security imaging," in *International Conference on Infrared, Millimeter, Terahertz Waves, IRMMW-THz* (IEEE, 2014), Vol. 1, p. 1.

[62]Y. Zhu, P. R. Byreddy, K. K. O, and W.-Y. Choi, "426-GHz imaging pixel integrating a transmitter and a coherent receiver with an area of $380 \times 470 \mu m2$ in 65-nm CMOS," in *IEEE Symposium on VLSI Circuits*, *Kyoto, Japan* (IEEE, 2019), pp. C18–C19.

[63]P. R. Byreddy, Y. Zhu, H. S. Bakshi, K. K. O, and W. Choi, "287-GHz CMOS transceiver pixel array in a QFN package for active imaging," in *2020 IEEE Asian Solid-State Circuits Conference (A-SSCC)* (IEEE, 2020), pp. 1–4.

[64]K. K. O, W. Choi, Y. Zhu, and H. Guo, "CMOS platform for everyday applications using sub-millimeter electromagnetic waves," IEEE Open J. Solid-State Circuits Soc. **2**, 1 (2022).

[65]R. W. McMillan, "Terahertz imaging, millimeter-wave radar," in *Advances in Sensing with Security Applications*, edited by J. Byrnes and G. Ostheimer (Springer, Netherlands, 2006), pp. 243–268.

[66]H. Saeidi, S. Venkatesh, C. R. Chappidi, T. Sharma, C. Zhu, and K. Sengupta, "A 4×4 distributed multi-layer oscillator network for harmonic injection and THz beamforming with 14dBm EIRP at 416 GHz in a lensless 65 nm CMOS IC," in *2020 IEEE International Solid-State Circuits Conference, ISSCC 2020* (IEEE, 2020), pp. 456–458.

[67]R. Shavit, A. Sabban, M. Sigalov, A. Lahman, Z. Iluz, N. Chayat, and S. Spiegel, "Microwave engineering research activity in Israel," IEEE Microw. Mag. **19**(3), 129–135 (2018).

[68]D. W. Bliss and K. W. Forsythe, "Multiple-input multiple-output (MIMO) radar and imaging: Degrees of freedom and resolution," in *Proceedings of 37th Asilomar Conference on Signals, Systems, Computers*, *Pacific Grove, CA* (IEEE, 2003), Vol. 1, pp. 54–59.

[69]J. Li, P. Stoica, and X. Zheng, "Signal synthesis and receiver design for MIMO radar imaging," IEEE Trans. Signal Process. **56**(8), 3959–3968 (2008).

[70]C. Tienda, J. A. Encinar, M. Arrebola, M. Barba, and E. Carrasco, "Member design, manufacturing and test of a dual-reflectarray antenna with improved bandwidth and reduced cross-polarization," IEEE Trans. Antennas Propag. **61**(3), 1180–1190 (2013).

[71]P. Nayeri *et al.*, "Beam-scanning reflectarray antennas," IEEE AP Mag. **57**(4), 32–47 (2015).

[72]J. Lien, N. Gillian, M. E. Karagozler, P. Amihood, C. Schwesig, E. Olson, H. Raja, and I. Poupyrev, "Soli: Ubiquitous gesture sensing with millimeter wave radar," ACM Trans. Graph. **35**(4), 1 (2016).

[73]Z. Hu, C. Wang, and R. Han, "A 32-unit 240-GHz heterodyne receiver array in 65-nm CMOS with array-wide phase locking," in *2018 RFIC Symposium, RTU1B-4* (IEEE, 2018), pp. 252–255.

[74]T. Chi, H. Wang, M.-Y. Huang, F. F. Dai, and H. Wang, "A bidirectional lens-free digital-bits-In/-Out 0.57mm2 terahertz nano-radio in CMOS with 49.3 mW peak power consumption supporting 50 cm internet-of-things communication," in *IEEE Custom Integrated Circuits Conference* (IEEE, 2017).

[75]P. R. Byreddy, W. E. Sosa, Y. Zhu, Z. Chen, B. Pouya, W. Y. Choi, and K. K. O, "Lens-less short-range reflection-mode imaging at 275 GHz using CMOS concurrent transceivers," IEEE Sens. Lett. **7**, 3500204 (2023).

[76]C. Wang and R. Han, "17.6 rapid and energy-efficient molecular sensing using dual mm-wave combs in 65 nm CMOS: A 220-to-320 GHz spectrometer with 5.2 mW radiated power and 14.6-to-19.5 dB noise figure," in *2016 IEEE International Solid State Circuits Conference*, *San Francisco, CA* (IEEE, 2016), pp. 426–427.

[77]Q. Zhong, Z.-Y. Chen, N. Sharma, S. Kshattry, W. Choi, and K. K. O, "300-GHz CMOS QPSK transmitter for 30-gbps dielectric waveguide communication," in *78 IEEE Custom Integrated Circuits Conference, Paper 13-4, San Diego, CA* (IEEE, 2018).

[78]P. Chevalier, W. Liebl, H. Rucker, A. Gauthier, D. Manger, B. Heinemann, G. Avenier, and J. Bock, "Sige BiCMOS current status and future trends in Europe," in *2018 IEEE BiCMOS and Compound Semiconductor Integrated Circuits and Technology Symposium* (IEEE, 2018), pp. 64–71.